Pergamon

0301-9322(94)E0006-5

Int. J. Multiphase Flow Vol. 20, No. 5, pp. 939–956, 1994

0301-9322/94 $7.00 + 0.00

LIQUID LAYER CHARACTERISTICS IN STRATIFIED–ATOMIZATION FLOW

S. V. PARAS, N. A. VLACHOS and A. J. KARABELAS†

Chemical Process Engineering Research Institute and Department of Chemical Engineering, Aristotle University of Thessaloniki, University Box 455, 54006 Thessaloniki, Greece

(Received 8 August 1993; in revised form 18 January 1994)

Abstract—Measurements of liquid film thickness, liquid-to-wall shear stress, pressure drop and visual observations have been carried out in a 50.8 mm i.d. horizontal pipe flow loop. Attention was paid to the lateral variation of the liquid properties by making measurements at locations $\Theta = 0°$ (pipe bottom) and $\Theta = 45°$

Statistical analysis of liquid film records led to the determination of local mean thickness, RMS values as well as of other wave characteristics (wave amplitude, intermittency, etc.) useful in computing gas–liquid interface friction. These data were complemented by similar statistical information from the shear stress measurements. The gas–liquid interface was found to deviate significantly from the usually assumed flat profile. A new result obtained here is that a small film thickness is associated with reduced local shear stress; i.e. that a lateral mean shear stress variation exists in this flow regime. In general, larger intensities of wall stress fluctuations are measured in thin films; e.g. at $\Theta = 45°$ as compared to $\Theta = 0°$ (thicker film).

Power spectra of film thickness and of shear stress display similarities indicative of the effect of waves on wall stress. There is also evidence suggesting that damping of interfacial waves takes place in relatively thick films. Probability densities of local layer thickness and of wall stress exhibit striking similarities indicative of a substrate on which a moving wavy layer develops.

Using the above new data, improved estimates of the interfacial friction factor f_i are obtained. The data exhibit a linear dependence of f_i on the liquid layer Reynolds number, as in previous studies. An expression relating an equivalent interface roughness to wave characteristics is also proposed.

Key Words: stratified–atomization flow, liquid layer thickness, liquid–wall stress, interfacial drag, pressure drop

INTRODUCTION

At gas velocities of the order of 10 m/s, and relatively small liquid flow rates, wavy stratified flow prevails in horizontal pipes, characterized by large amplitude roll waves otherwise known as Kelvin–Helmholtz waves (Andritsos & Hanratty 1987). At still higher gas velocities, liquid droplets (a typical feature of annular flow) appear throughout the gas phase, evidently torn off from the crests of these large amplitude waves. Thus, the region in figure 1 identified as "atomization" represents a transition regime from stratified to annular flow even though it is usually viewed as part of stratified flow.

The stratified–atomization flow regime is easier to study experimentally than the more complex annular regime. Moreover, it exhibits some features (droplet entrainment, wavy liquid layer at the pipe bottom) which are common to both neighboring flow regimes. Therefore, data and models for stratified–atomization flow are expected to provide considerable guidance, and to serve as the basis, for modeling (at least some aspects of) the more complicated annular flow regime. As regards applications, the stratified–atomization regime frequently prevails in long distance pipelines (e.g. Wu *et al.* 1987) and in process plants. Furthermore, many practical problems (e.g. corrosion and scaling in two-phase pipelines, friction losses) are mainly influenced by the characteristics of the liquid layer at the wall. Better understanding and control of the liquid layer would result in more effective measures to tackle such problems.

It is the purpose of this work to study the characteristics of the liquid layer in stratified–atomization flow, paying attention to the circumferential variation of film properties.

†To whom all correspondence should be addressed.

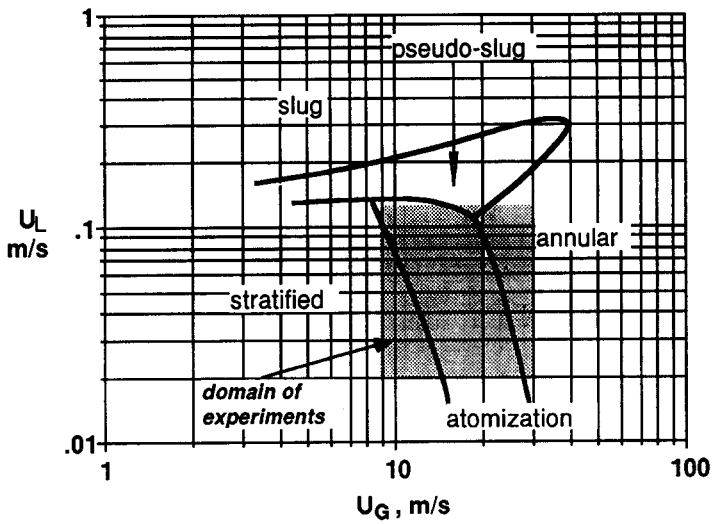

Figure 1. Flow map (Paras & Karabelas 1991) and domain of experiments.

Therefore, instantaneous film thickness and wall shear stress measurements were made at two locations, i.e at $\Theta = 0°$ (pipe bottom) and $\Theta = 45°$, combined with pressure drop data and visual observations. By analyzing these measurements useful information was obtained concerning the flow within the film as well as the gas–liquid interface waviness and friction.

Although several related studies have appeared in the literature in recent years, stratified pipe flow with relatively thin liquid films has not been adequately researched. Andritsos & Hanratty (1987) reviewing available models (with emphasis on gas–liquid interfacial stress computations) point out the main drawbacks. Two of them in presently used computational procedures are the neglect of the possible lateral variation of local shear stress or local velocity close to the pipe wall and the assumption of a velocity profile applicable to full pipes. However, recent velocity measurements (Paras & Karabelas 1992) suggest that the universal velocity profile is not applicable to relatively thin liquid layers and that the effect of disturbance waves on film flow characteristics is dominant.

The paper by Kowalski (1987) is apparently the only place where shear stress data are presented for stratified flow in pipes. Using hot film probes, Kowalski made wall shear stress measurements on the liquid side as well as similar measurements at the gas–wall interface. He also measured Reynolds shear stresses in the gas phase. Relatively low gas velocities were employed in these tests. Using a flow momentum balance and the above measurements, empirical correlations were developed for predicting the interfacial friction factor.

Hagiwara *et al.* (1989) conducted experiments in a 49.4 mm i.d. horizontal tube in order to examine the influence of large interface waves on wall shear stress. Simultaneous measurements were made of wall shear stress, liquid film thickness and streamwise gas velocity. It was suggested that a separation bubble is attached to the front of the large waves. It was also observed that an increase in the wall shear stress is caused by passing large waves. Otherwise, no mean shear stress data were reported.

Gas–liquid interaction in a channel of rectangular cross section was studied by Miya *et al.* (1971). Roll waves were modeled on the basis of simultaneous liquid–wall shear stress, film thickness and pressure measurements. The influence of roll waves on wall shear stress was documented. Of interest to this study is the observed linear dependence of gas–liquid interface friction factor f_i on the liquid Reynolds number. This correlation is occasionally used (e.g. Cheremisinoff & Davis 1979) in horizontal stratified pipe flow as well.

Of some relevance to this work are wall shear stress data, for vertical two-phase flow, reported by Govan *et al.* (1989) and Martin & Whalley (1983). The latter observed again a direct influence of large waves on shear stress, with a small time delay.

Hart *et al.* (1989) carried out experiments in a horizontal 51 mm i.d. pipe, with small liquid holdup values, in stratified, wavy stratified and annular flow. They measured pressure drop and holdup and developed a model for predicting these quantities. Of special interest to this work is a correlation they propose to estimate the portion of the circumference (in the lower part of the pipe) wetted by the continuous liquid layer.

In the following section the experimental techniques are outlined. The main results on film thickness and shear stress characteristics are presented next, followed by predictions of gas–liquid interfacial friction.

EXPERIMENTAL TECHNIQUES

The experiments were carried out in a horizontal flow loop described in a paper by Paras & Karabelas (1991). Stratified–atomization flow developed in a 16 m long straight section, of 50.8 mm i.d. The test section is positioned about 300 dia downstream of the mixing section of the two phases where the flow is considered to be fully developed. The selected range of superficial velocity, was 2–12 cm/s for water and 10–30 m/s for air (denoted by U_L and U_G respectively). The experiments were carried out very near atmospheric pressure.

Wave heights and liquid film thickness along the pipe in two-phase flow are measured using parallel wire conductance probes. The technique is based on the fact that the conductance between two parallel wires is uniquely related to the liquid level between them.

Two Plexiglas test sections were designed and constructed for film thickness measurements as described in detail elsewhere (Paras & Karabelas 1991). Two parallel wire conductance probes were placed in the first test section at $\Theta = 0°$ and $\Theta = 45°$, from the pipe bottom, for the thin film measurements. In fabricating such a probe, a special cylindrical Plexiglas plug was machined, to be flush with the inside pipe wall when mounted onto the test section. Each probe had two parallel chromel wires 0.5 mm in dia, 2.5 mm apart with a 12 mm length exposed to flow. The two wires were embedded almost radially on the same pipe cross section. A second test section was constructed to accommodate three probes at $\Theta = 0°$ and at relative distances $\Delta x = 3$, 9 and 12 cm. The wires in this case were long, covering the entire pipe diameter. This test section was used for thick film measurements at the pipe bottom. Prior to and after each run measurements of water conductivity were made in order to eliminate the effect of temperature on the wire probe conductance. Simultaneous measurements with these probes were employed to compute cross-correlation functions and to estimate wave celerities. The probes are part of an electronic circuit, with the main components a custom-made analyzer–demodulator and a function generator supplying a 25 kHz carrier signal. The DC output from the analyzer corresponds to the film height (Paras & Karabelas 1991).

Another type of probe can be located 4 cm upstream of the parallel wire probes, on the first section, for performing wall shear stress measurements. The sensors for such measurements are flush-mounted hot-film probes (DANTEC 55R46), calibrated by measuring the voltage output in a single-phase water flow field. The wall shear stress (τ_{wL}) in such a system is predicted by well-known expressions and can be related to the measured voltage (V) as follows:

$$V^2 = A\,(\tau_{wL})^{1/3} + B$$

where A and B are constants depending on the temperature (e.g. Kowalski 1987) and determined by calibration. The output voltage from the anemometer is corrected for temperature variations during the experiments. The maximum error due to temperature is expected to be less than 6% since the temperature variation during the tests is less than 2%.

The inner surface of the test sections, although not polished after machining, was very smooth and easily wetted. However, the effect of wettability was not considered in these experiments.

Pressure drop measurements were made using a differential pressure transducer (variable reluctance pressure transducer, Validyne). The two pressure taps, which are located at the pipe bottom, are 3.9 m apart, with the first tap being 240 dia downstream of the mixing section. In order to avoid air bubbles in the tubes connecting the pressure transducer, care was taken to purge those lines frequently.

Table 1. Summary of experimental conditions and liquid layer results

Run	U_L (cm/s)	U_G (m/s)	h_0	h_{RMS0} (mm)	h_{45}	h_{RMS45}	ε_L (%)	f_0 (Hz)	h_w (mm)	I (—)
A	1.9	11.5	3.69	1.12	0.27	0.06	4.2	1	7.3	0.05
B	1.9	16.5	2.34	1.14	0.34	0.07	3.0	4	5.0	0.23
C	1.9	22.1	1.56	0.91	0.33	0.09	2.2	7	3.9	0.31
D	1.9	29.7	0.74	0.47	0.28	0.10	1.3	9	2.1	0.30
E	3.1	11.6	4.90	1.34	0.43	0.12	5.7	1	8.4	0.07
F	3.1	16.2	3.33	1.46	0.40	0.10	4.1	3	7.2	0.12
G	3.1	21.9	2.26	1.27	0.38	0.10	3.0	5	5.5	0.18
H	3.1	29.5	1.22	0.75	0.33	0.11	1.9	7	3.1	0.34
I	5.9	11.4	6.70	1.80	0.62	0.17	7.8	1	11.2	0.08
J	5.9	16.3	4.81	1.93	0.50	0.13	5.7	2	9.1	0.15
K	5.9	21.3	3.53	1.71	0.46	0.13	4.4	3	7.4	0.18
M	9.0	11.3	8.11	2.45	0.75	0.20	9.5	1	13.8	0.07
N	9.0	16.0	6.07	2.32	0.60	0.16	7.2	2	11.0	0.12
Q	12.1	11.1	9.29	2.82	0.84	0.24	10.8	1	15.5	0.11
R	12.1	15.9	6.90	2.72	0.68	0.19	8.1	2	12.4	0.16
A1	10.0	11.9	7.60	2.60	0.78	0.22	9.0	1	14.0	0.08
B1	8.0	11.9	6.50	2.20	0.70	0.18	7.8	1	13.1	0.07
C1	4.0	11.9	4.40	1.50	0.50	0.14	5.3	1	9.7	0.07
D1	2.5	11.9	3.40	1.10	0.36	0.09	4.1	1	7.3	0.05

Visual observations were made using an angle gauge to measure the angle θ over which the tube was wetted by the continuous liquid phase at the pipe bottom, with an estimated accuracy of $\pm 3°$.

The analog output from the analyzer, the anemometer unit and the pressure transducer were fed to a 12 bit A/D converter (DT 2801-A, Data Translation Inc.) and recorded by a PC 486 compatible, using a computer code developed in our laboratory.

Data sets used for obtaining film thickness, pressure drop and shear stress statistical information (mean, RMS etc.) were collected for a period of 32 s with a sampling frequency of 250 Hz. In order to estimate the dominant frequencies associated with the stratified–atomization regime, using the spectral density function, data sets were recorded and stored for a period of 5 min with a sampling frequency of 100 Hz. Finally, data for wave celerity calculations, using the cross-correlation function, were sampled for 16.5 s with a sampling frequency of 500 Hz.

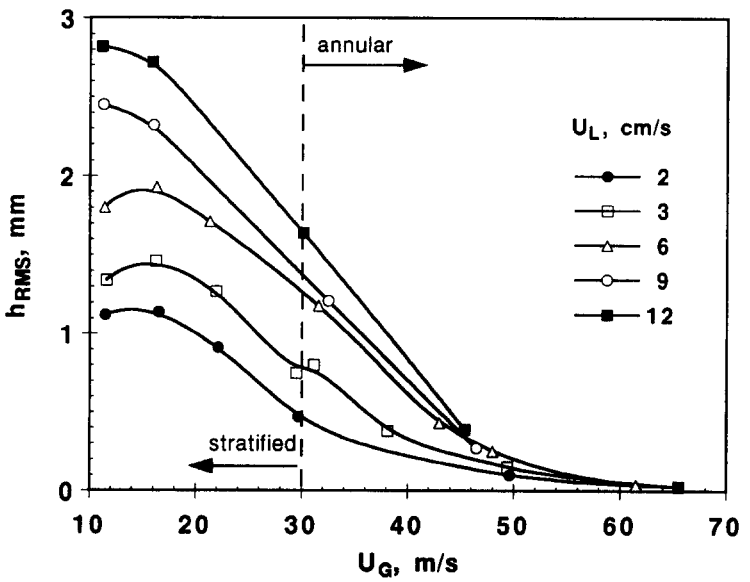

Figure 2. The effect of superficial gas and liquid velocity on RMS values of film thickness.

RESULTS

Film thickness data

Table 1 summarizes flow conditions and time-averaged film thickness data. Additionally, liquid holdup (ε_L) and large wave height (h_w), frequency (f_0) and intermittency (I) are included therein. Subscripts 0 and 45 represent the pipe bottom and a circumferential location 45° from the bottom, respectively. The velocities U_L and U_G are superficial.

Statistical analysis of film records has allowed the study of variation of time-averaged thickness, of RMS values and of other quantities. As expected, the mean film thickness at the pipe bottom ($\Theta = 0°$) tends to decrease with increasing gas velocity. The RMS value of the film thickness varies with both superficial liquid and gas velocities, as shown in figure 2. It is evident that by increasing gas velocity the RMS value decreases rapidly, whereas it increases with liquid velocity. The data for annular flow presented in figure 2, and in some subsequent figures, were obtained in the same experimental setup earlier (Paras & Karabelas 1991). They are included here to check for consistency and to examine general trends. The discontinuity displayed by one data set ($U_L = 3$ cm/s) at $U_G \approx 30$ m/s in figure 2 as well as in the following figure 9, is attributed to

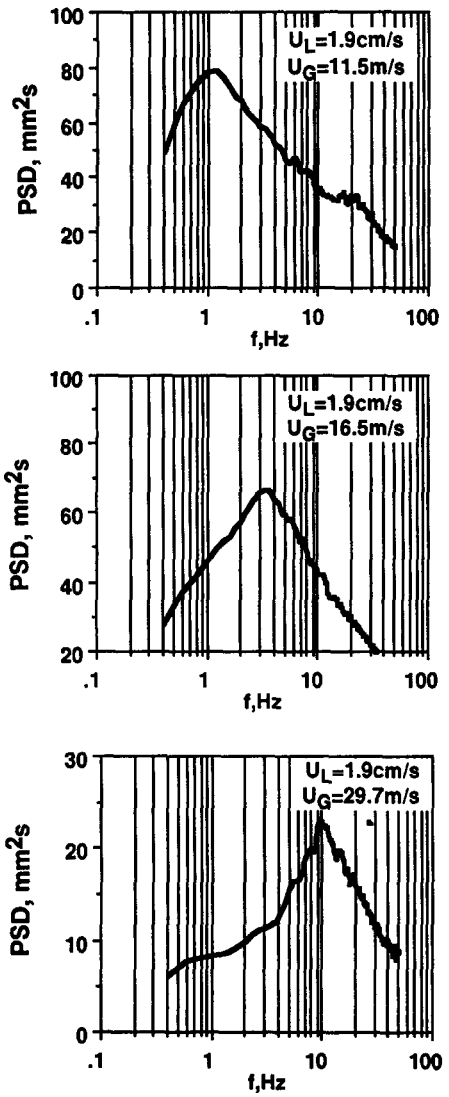

Figure 3(a). Power spectra of film thickness for various gas flow rates and a relatively low liquid flow rate ($U_L = 1.9$ cm/s) at the pipe bottom ($\Theta = 0°$).

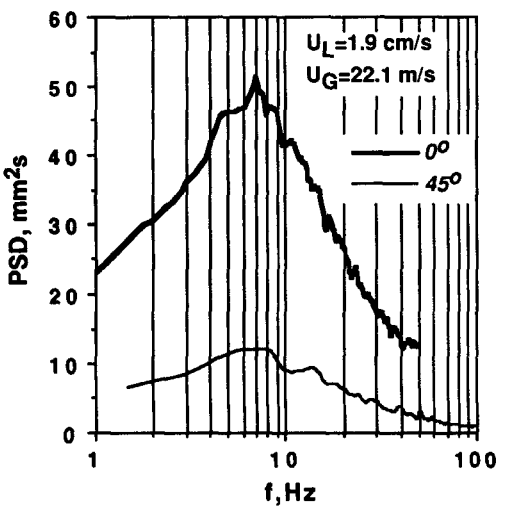

Figure 3(b). Power spectra of film thickness for experiment C at $\Theta = 0°$ and 45°; ($U_L = 1.9$ cm/s, $U_G = 22$ m/s).

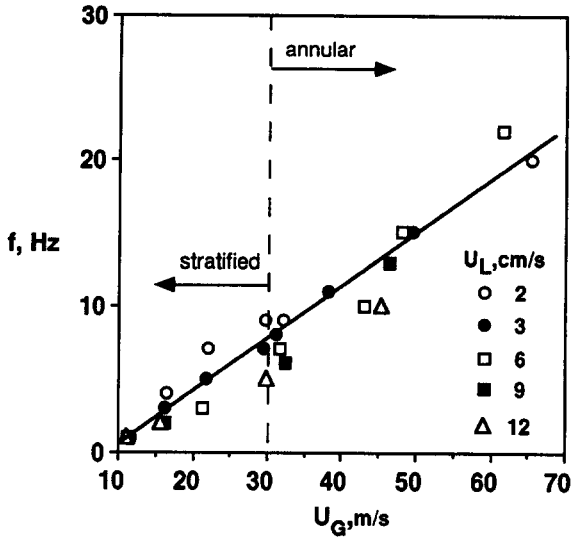

Figure 4. The effect of gas velocity on the characteristic wave frequency, for various liquid velocities.

experimental errors since the measurements in annular flow were taken earlier (Paras & Karabelas 1991) with slightly different test conditions.

The power spectra of the film height time series were obtained by the Welch method (averaging modified periodograms). There was a 50% overlap between successive data segments each having 512 data points. The data were modified by a Parzen window before computing the periodogram. A 5-point smoothing procedure was performed on the final periodogram. According to Bendat & Piersol (1986), the resulting standard error in the final estimation was 4.5%.

It is observed that at relatively small gas velocities (U_G up to 17 m/s) the dominant frequency is between 1 and 3 Hz, but at higher gas velocities ($U_G > 20$ m/s) it is shifted in the range 5–10 Hz. In general, the dominant frequency displays a tendency to increase with gas flow rate, as shown in figure 3(a). Similar PSD plots, not presented here, show that the dominant frequency is rather insensitive to changes of the liquid flow rate. Power spectra of film thickness corresponding to $\Theta = 0°$ and 45°, for flow conditions well within the atomization regime, are included in figure 3(b). The dominant frequency is essentially the same in both locations suggesting that it is due to the

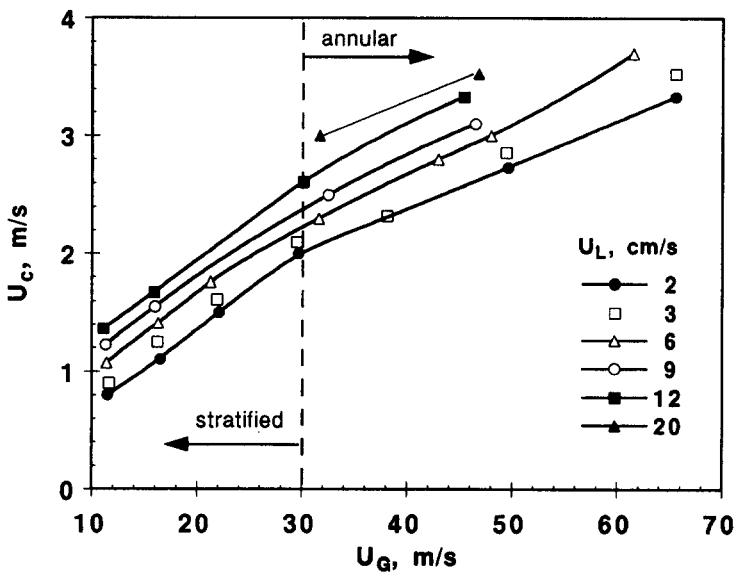

Figure 5. Wave celerity as a function of gas and liquid flow rate.

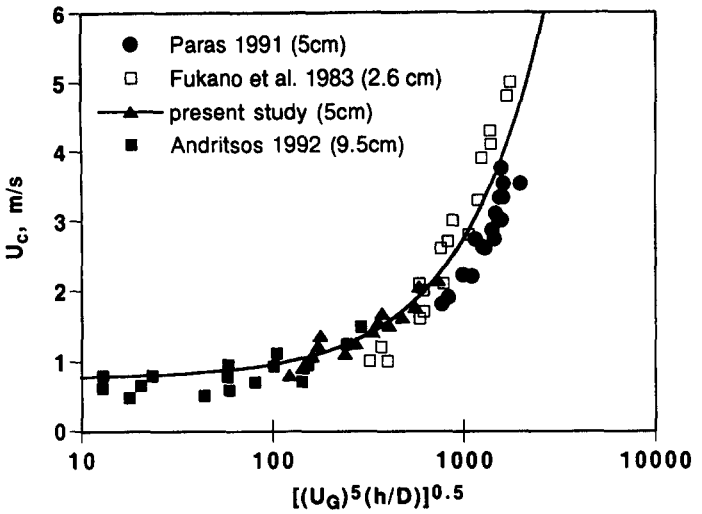

Figure 6. Correlation of wave celerity: $U_c = 0.75 + 0.002\,[U_G^5(h_0/D)]^{0.5}$; data from various studies.

same large waves. It will be pointed out here that, upon close examination of figure 3(a), it is evident that a class of waves of frequency around 1 Hz persists, even at relatively high gas velocities (e.g. $U_G = 16.5$ m/s) although their amplitude has been reduced. These waves may be associated with the Kelvin–Helmholtz instability. The origin of higher frequency waves, dominating at higher gas velocities, is difficult to ascertain at present, although they have the appearance of irregular roll waves originally observed by Hanratty & Engen (1957).

All the dominant wave frequency data obtained in our experimental setup are presented in figure 4. An almost linear dependence of the characteristic frequency on gas velocity is evident, whereas the influence of liquid velocity appears to be of less significance.

Wave celerities were obtained by calculating the cross-correlation function of two simultaneously recorded signals from locations at a distance $\Delta x = 9$ cm. Figure 5 shows that wave celerity increases markedly with the gas as well as with the liquid velocity. The nearly linear dependence of wave celerity on gas velocity shown in figure 5, is also observed in the data of Andritsos (1992) for smaller gas velocities. In figure 6 an attempt is made to correlate wave celerity data from various tests and pipe diameters $D = 2.6$, 5.0 and 9.5 cm. From this figure one may draw the conclusion that U_c (m/s) data are fitted fairly well with an expression involving superficial gas velocity U_G (m/s) and the ratio of mean film thickness at the bottom of the pipe h_0 (mm) and pipe diameter D (mm). With such an expression one could correlate data from other studies as well; e.g. Fukano *et al.* (1983) and Andritsos (1992).

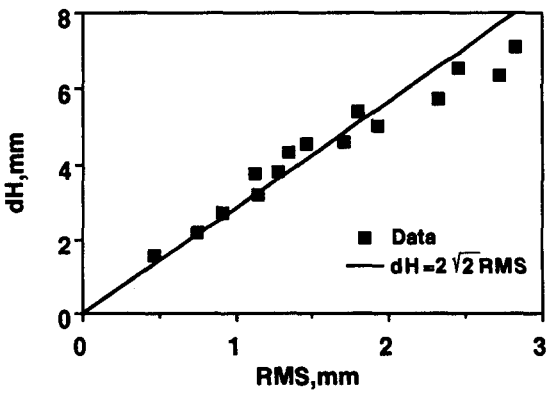

Figure 7. Correlation of large wave amplitude as a function of RMS values of film thickness.

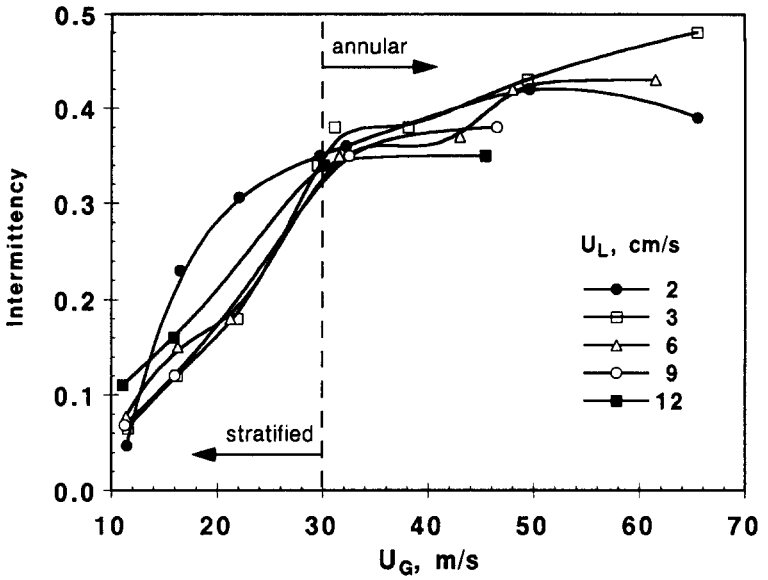

Figure 8. Large wave intermittency as a function of gas and liquid superficial velocity.

The mean large wave amplitude dH is found to be a linear function of the RMS value of the film height (figure 7); i.e. $dH = 2\sqrt{2}$ (RMS). It is interesting that this type of expression (representative of sinusoidal wave motion) is applicable to irregular large waves as well.

Large wave intermittency, defined as the fraction of total sampling time corresponding to the passage of large waves is useful in the description of processes (such as atomization) occurring at the gas–liquid interface (Schadel 1988). The approach followed for determination of the large wave intermittency as well as its amplitude and length is described elsewhere (Paras & Karabelas 1991). The analysis has produced some interesting results in stratified–atomization flow; i.e. for $U_G < 30$ m/s large wave intermittency increases with gas velocity whereas it is almost independent at gas velocities above 30 m/s (annular flow), having a value between 0.3 and 0.4 as shown in figure 8. This quantity appears to be a weak function of liquid velocity. Increased intermittency is associated with an increased rate of liquid atomization.

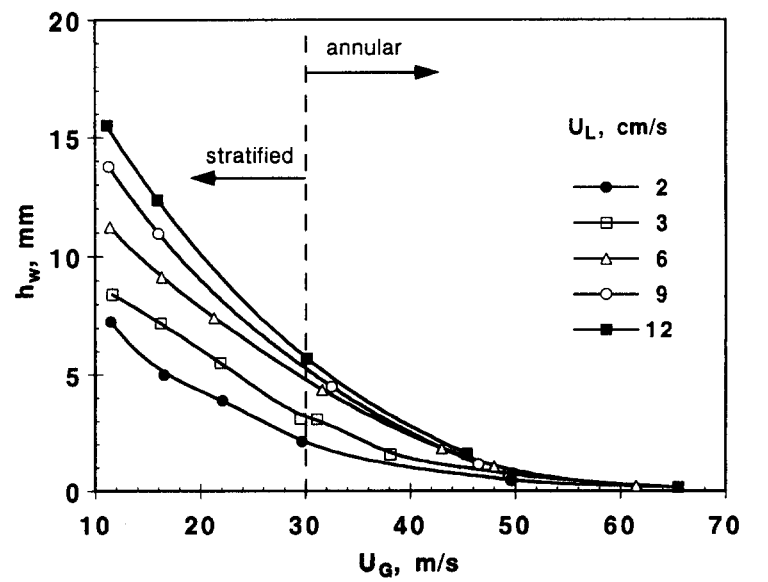

Figure 9. The influence of gas and liquid superficial velocity on large wave height.

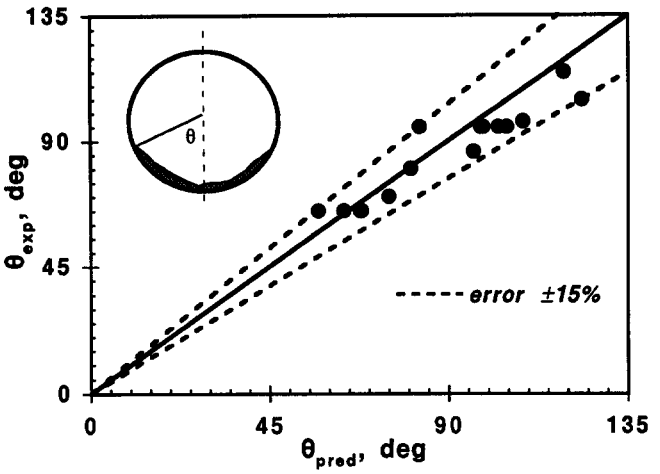

Figure 10. Wetted wall fraction data against predicted values using the Hart *et al.* (1989) correlation.

Figure 9 shows the strong influence of gas flow rate on the large wave height. The influence of superficial liquid velocities on the large wave height is significant in stratified–atomization flow, but tends to be reduced in annular flow, becoming insignificant above $U_G \approx 50$ m/s.

Wetted wall fraction

The observed values of the wetted wall fraction in terms of the angle θ are in good agreement with the calculated values from a model proposed by Hart *et al.* (1989)—their equation [13]—as shown in figure 10. Values of wetted wall fraction, combined with the independently measured mean film thickness at $\Theta = 0°$ and 45°, enable one to estimate the time-average profile of the gas–liquid interface as well as the liquid holdup ε_L. Data for the latter included in table 1.

As expected, with increasing gas velocity the area of the interface tends to increase and to deviate significantly from the flat (time-averaged) shape, assumed in presently used computational procedures.

Shear stress data

Time-averaged shear stress, and the respective RMS values, together with the time-averaged film thickness and two-phase pressure drop data are included in table 2. These data are somewhat arbitrarily classified in two categories, i.e. for relatively thin and thick layers, to facilitate their

Table 2. Time-averaged film thickness, wall shear stress and pressure drop data

Run	U_L (cm/s)	U_G (m/s)	h_0 (mm)	h_{45}	τ_{wL0}	τ_{wL45}	τ_{RMS0} (N/m^2)	τ_{RMS45}	dp/dx (N/m^3)	
D	1.9	29.7	0.74	0.28	16.58	15.18	9.03	12.08	473	annular
H	3.1	29.5	1.22	0.33	14.78	16.37	9.40	12.80	622	flow
C	1.9	22.1	1.56	0.33	12.44	7.20	4.96	6.58	245	
G	3.1	21.9	2.26	0.38	13.20	7.65	5.04	8.35	290	
B	1.9	16.5	2.34	0.34	10.00	3.44	3.93	3.60	136	"thin"
F	3.1	16.2	3.33	0.40	7.81	4.82	3.99	4.46	162	films
D1	2.5	11.9	3.40	0.36	2.58	2.13	0.79	1.67	68	
K	5.9	21.3	3.53	0.46	12.93	9.11	5.07	9.25	367	
A	1.9	11.5	3.69	0.27	2.07	1.00	1.19	1.09	64	
C1	4.0	11.9	4.40	0.50	3.72	3.84	1.91	2.71	85	
J	5.9	16.3	4.81	0.50	8.67	6.10	3.37	4.73	199	
E	3.1	11.6	4.90	0.43	3.37	3.05	1.17	2.25	75	
N	9.0	16.0	6.07	0.60	7.31	6.84	2.60	5.27	242	"thick"
B1	8.0	11.9	6.50	0.70	4.91	5.15	1.45	2.80	125	films
R	12.1	15.9	6.90	0.68	9.64	7.07	3.62	5.78	285	
A1	10.0	11.9	7.60	0.78	6.48	5.50	3.56	2.93	140	
M	9.0	11.3	8.11	0.75	3.41	3.69	1.44	3.14	135	
Q	12.1	11.1	9.29	0.84	5.27	5.78	2.47	2.93	161	

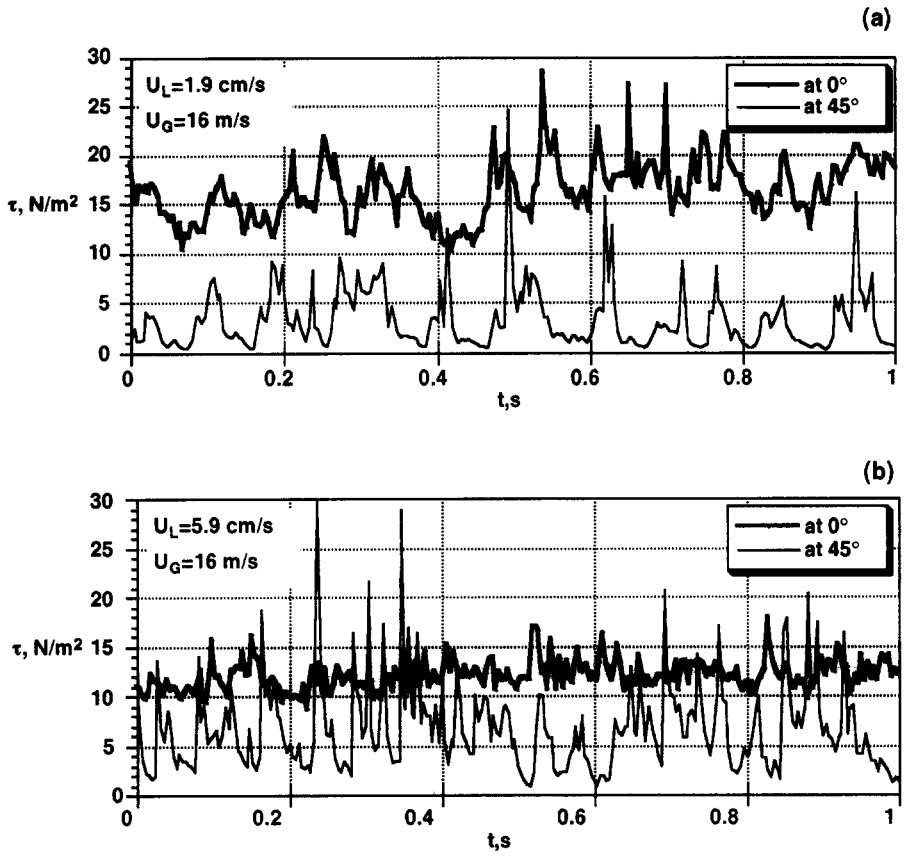

Figure 11. Typical traces of wall shear stress: (a) relatively thin film and (b) relatively thick film.

interpretation. Two other points at high gas velocities (runs D and H) were visually observed to belong to the annular flow regime.

An inspection of the h_0 and h_{45} data in table 2, combined with the independent visual observations, reveal that (especially in the case of thin films) the form of the time-averaged gas–liquid interface is concave; i.e. quite different than the usually assumed (for stratified flow) flat shape. It is also observed visually, and in film thickness traces, that there are no dry patches on the wetted portion of the pipe wall and that a continuous film (occasionally very thin, however) covers the lower part of the circumference. Typical shear stress traces are included in figure 11. These time series were recorded under the same flow conditions but not simultaneously. The traces in figure 11(a) correspond to a "thin" film and those of figure 11(b) to a "thick" one. The sharp peaks in both cases appear to be caused by gas–liquid interface waves influencing flow conditions at the pipe surface.

Interesting trends are noted by comparing time-averaged and RMS values of shear stress. For relatively thin liquid layers ($h_0 < 4$ mm) the time-averaged stress at 45° is considerably smaller than at the bottom. One likely interpretation is based on the fact that the film at 45° is very thin, intermittently immobile with respect to air flow and thus associated with very small values of instantaneous shear stress. It is further noted in table 2 (for thin films) that at 45° the time-averaged stress and the respective RMS are roughly equal, indicating that the waves in the vicinity of 45° penetrate the liquid layer down to the solid wall.

In the case of relatively thick liquid films ($h_0 > 4$ mm) the mean shear stress at 45° is roughly equal or quite close to the stress at the bottom, which is indicative of a sufficient film thickness at 45°. Run R does not follow this trend, but it appears to belong in the "pseudo-slug" and not in the stratified–atomization flow regime. In line with the above observation is the fact that at 45° the RMS value is smaller than the corresponding time-averaged stress, as is also the case with the

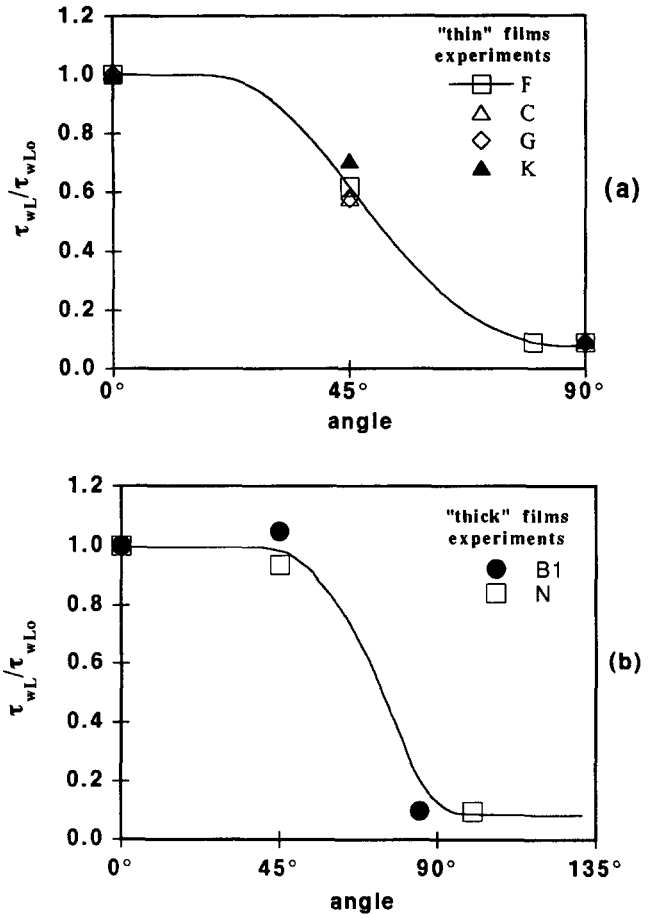

Figure 12. Circumferential distribution of normalized τ_{wL} with respect to its value at $\Theta = 0°$: (a) relatively thin films and (b) relatively thick films.

0° data. This suggests that the influence of interfacial waves on τ_{wL} is greater in the relatively thinner films.

Two runs (D and H, table 2) belonging to the annular regime exhibit the highest average and RMS shear stresses. Moreover, the average τ_{wL} values at 0° and 45° in these runs are nearly equal due to the very high gas velocities.

The variation of the liquid–wall shear stress around the circumference of the pipe normalized with respect to the value at the pipe bottom (τ_{wL0}) is shown in figure 12 for both "thin" and "thick" films. It is observed that for relatively thick films the region of nearly constant wall stress is larger compared to that for thin films. Thus, one is led to the conclusion that for relatively "thick" films τ_{wL} may be almost constant up to a point where an adequate film thickness exists. Beyond that point, the smaller liquid film thickness is associated with a reduced wall shear stress. The value of τ_{wL} at an angle θ (corresponding to the wetted wall fraction) is considered equal to the gas-to-wall shear stress, since no liquid film exists above that angle. The latter is calculated using [4] given below.

Interesting observations can be made by comparing the spectral densities of fluctuating film thickness (figure 3) with those of shear stress (figure 13). It is clear that for relatively thick films, usually encountered at the pipe bottom [e.g. figure 3(a), $U_G = 11.5$ m/s and figure 13(b)] the two types of spectra are similar exhibiting only low characteristic frequencies ($f \approx 1$–2 Hz) which may be attributed to the same class of large waves. For relatively thin films (i.e. at $\Theta = 45°$) an additional pronounced frequency peak is observed in the shear stress spectrum between 5 and 10 Hz [e.g. figure 13(a)], which corresponds to the high frequency part of the thickness spectrum [e.g. figure 3(b)]. A similar observation can be made in the shear stress spectra of Martin & Whalley (1983) although

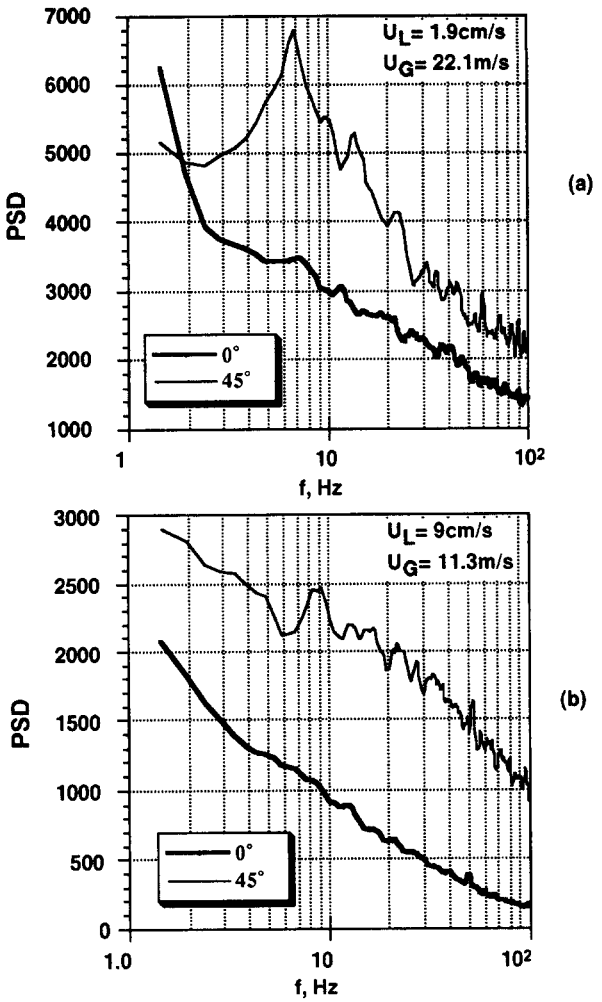

Figure 13. Typical spectra of wall shear stress at $\Theta = 0°$ and 45°: (a) relatively thin film and (b) relatively thick film.

the latter were obtained in vertical annular flow. Furthermore, the spectra of axial velocity within the liquid layer reported recently (Paras & Karabelas 1992—their figure 12 (a) and (b)) also display this second peak, at 5–10 Hz, close to the interface indicative of a class of waves. A possible interpretation of all the above evidence is that waves of somewhat smaller amplitude, in the frequency range 5–10 Hz, can affect local velocities at the wall and shear stress only in the case of relatively thin films. In thicker films the influence of such waves does not extend down to the pipe wall, being dampened by the liquid. On the contrary, the influence of low frequency large waves is evident in essentially all the data collected here, for relatively thin and thick liquid films; i.e. throughout the liquid layer.

New information regarding the close relationship between film thickness and shear stress is also provided by the respective probability density distributions. Figure 14 (a) shows that (at 45°) relatively thin liquid films exhibit a unimodal distribution perhaps associated with low velocity liquid reaching that particular lateral location. With increasing liquid flow rate and film thickness, the density distribution evolves into a bimodal one [figure 14 (b)–(d)]. The first peak, located between 0.3 and 0.4 mm, does not appear to be significantly affected by liquid flow rate and may represent a base layer in contact with the solid surface. The second peak, becoming more pronounced with increasing layer thickness, probably reflects the growing effect of large amplitude waves, travelling on the liquid substrate.

Striking similarities are observed in the corresponding shear stress probability density distributions for $\Theta = 45°$ (figure 15). A unimodal distribution for small film thickness appears at small

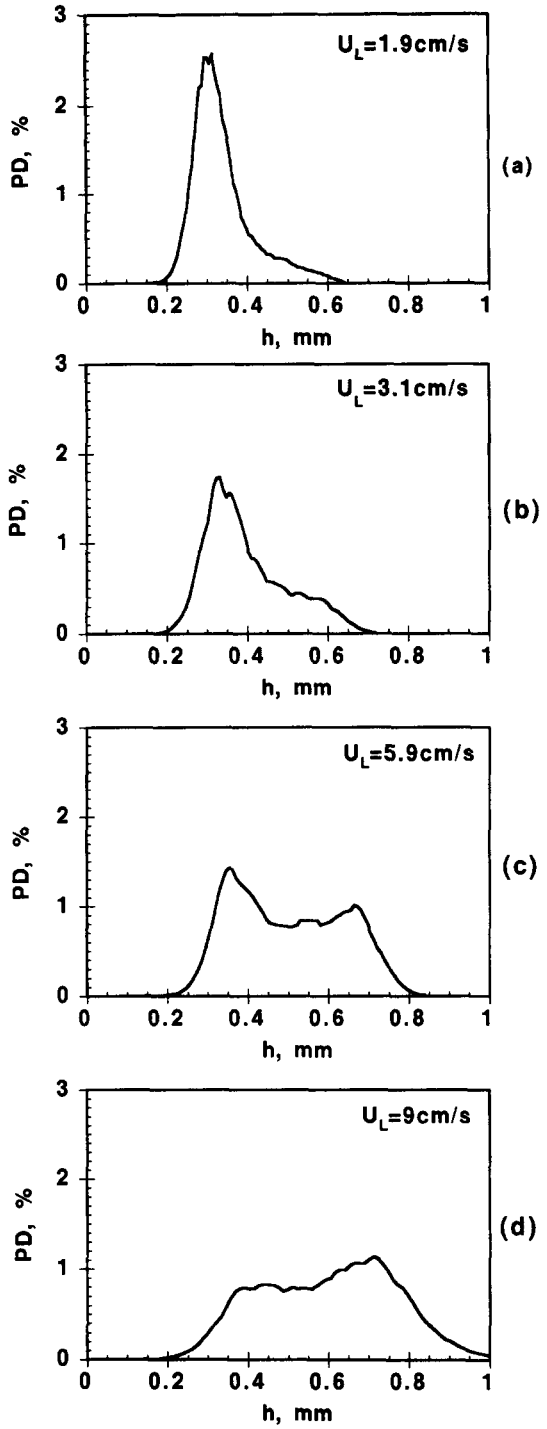

Figure 14. Typical probability density distributions of film thickness at $\Theta = 45°$ for constant $U_G = 16$ m/s and various liquid rates.

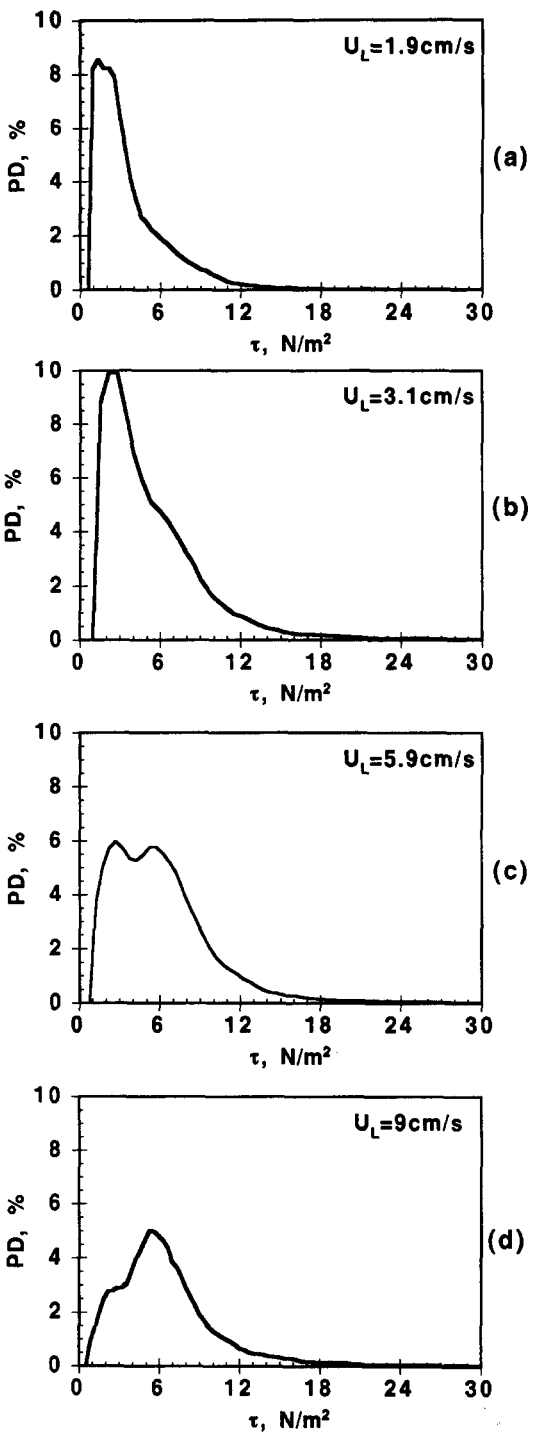

Figure 15. Typical probability density distributions of wall shear stress at $\Theta = 45°$ for constant $U_G = 16$ m/s and various liquid rates.

values of shear stress [figure 15 (a)], gradually evolving into a bimodal one with increasing liquid flow rate and thickness. This is considered as additional evidence that large amplitude waves tend to move on a gradually thickening substrate.

From the data reported here, average values of liquid-to-wall shear stress τ_{wL} are obtained and the corresponding friction factor f_L is computed. In figure 16 such data are plotted versus the liquid

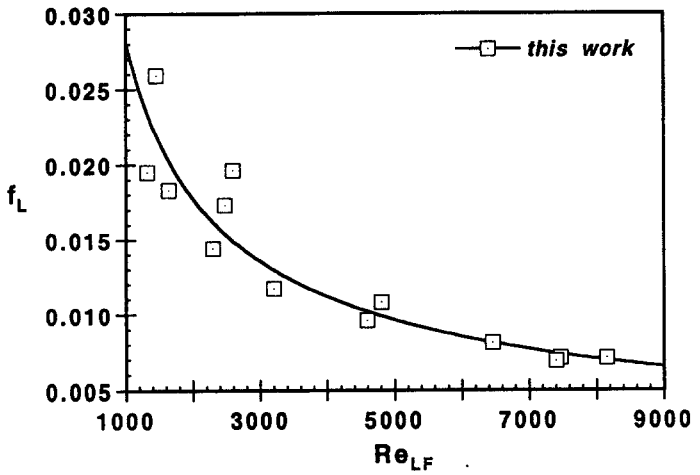

Figure 16. Wall-to-liquid friction factor data plotted vs the corresponding liquid Reynolds number.

Reynolds number Re_{LF}, based on real mean liquid velocity and mean liquid thickness at the bottom, h_0. A fairly good data correlation is obtained using the equation:

$$f_L = 2.86 Re_{LF}^{-2/3} \quad [1]$$

as shown in figure 16. Kowalski (1987) using a Reynolds number based on superficial velocity correlated his data with a similar expression, involving a -0.5 exponent instead of the -0.66 obtained here.

DETERMINATION OF INTERFACIAL FRICTION

The new data reported here on film thickness and shear stress, combined with better estimates of the gas–liquid interface shape and area, enable one to determine the interface shear stress with improved accuracy. This is achieved by means of the following expressions obtained from momentum balances (e.g. Taitel & Dukler 1976; Andritsos & Hanratty 1989) for the liquid and gas phase, respectively

$$-A_L\left(\frac{dp}{dx}\right) - \tau_{wL} P_L + \tau_i S_i = 0 \quad [2]$$

$$-A_G\left(\frac{dp}{dx}\right) - \tau_{wG} P_G - \tau_i S_i = 0 \quad [3]$$

where A_L, A_G, P_L, P_G, S_i, are defined in figure 17. As pointed out earlier, the assumption of a flat interface employed so far by various investigators (e.g. Agrawal *et al.* 1973; Andritsos & Hanratty 1987) is not valid in the flow regime examined here. Therefore, the above parameters are obtained from the measured values of film thickness and the visual observations of the wetted part of the circumference (angle θ). The interfacial area S_i is satisfactorily approximated by taking the straight line segment CD instead of the arc CD (figure 17).

The above equations represent a balance between the pressure forces on the liquid and gas phase and the resisting stresses at the liquid–wall and gas–wall boundary (τ_{wL} and τ_{wG}) and at the gas–liquid interface (τ_i). Having measured pressure drop (dP/dx), liquid film height and liquid–wall shear stress the product $\tau_i \cdot S_i$ can be obtained from [2]. An average value of the liquid–wall shear stress was taken using the measured values at 0°, 45° and the value at θ. The latter was considered to be equal to the stress exerted by the gas flow on the solid wall (τ_{wG}) since circumferentially the shear stress is continuous.

The gas–wall shear stress is given in terms of a friction factor (f_G) and the superficial gas velocity (U_G); i.e.

$$\tau_{wG} = f_G \frac{\rho_G U_G^2}{2} \quad [4]$$

where $f_G = 0.046\ \mathrm{Re}_G^{-0.2}$

The product $\tau_i \cdot S_i$ was also calculated by using [3] and very good agreement was obtained between the two values. Finally, an average value is taken in order to evaluate the interfacial shear stress. The latter is expressed in terms of an interfacial friction factor (f_i) as:

$$\tau_i = f_i \frac{\rho_G U_G^2}{2} \quad [5]$$

Our data for relatively low superficial gas velocities are in fairly good agreement with the empirical correlation for predicting interfacial friction factor in wavy stratified flow proposed by Kowalski (1987):

$$f_i = 7.5 \times 10^{-5}\ \varepsilon_L^{-0.25}\ \mathrm{Re}_G^{-0.3}\ \mathrm{Re}_L^{0.83} \quad [6]$$

where ε_L is the liquid holdup and Re_G and Re_L the gas and liquid Reynolds numbers respectively, based on the actual phase velocities and the pipe diameter. However, for relatively high superficial gas velocities this correlation does not perform well. This may be attributed to the fact that Kowalski's data (on which the correlation was based) were obtained under relatively small gas velocities compared to our measurements, i.e. below the atomization regime.

Quite often in studies of stratified flow (e.g. Cheremisinoff & Davis 1979) a linear expression is employed relating f_i to the liquid Reynolds number Re_{LF}, as originally suggested by Miya *et al.* (1971) for channel flow. Using the aforementioned procedure ([2]–[5]) we have plotted the f_i data versus Re_{LF} in figure 18. A satisfactory linearity is observed and the best fit is obtained from the expression:

$$f_i = 0.022 + 3.7 \times 10^{-6} \mathrm{Re}_{LF} \quad [7]$$

where

$$\mathrm{Re}_{LF} = \frac{U_L h_0}{\varepsilon_L \nu_L}$$

Data by Andritsos (1986) close to the range of our measurements are also plotted in figure 18. These data are obtained by recalculating S_i and P_L, using the correlation by Hart *et al.* (1989) to estimate the angle θ (figure 17) and the respective wetted part of the circumference. The agreement with our data is considered satisfactory. A correlation such as [7] does take into account the effect

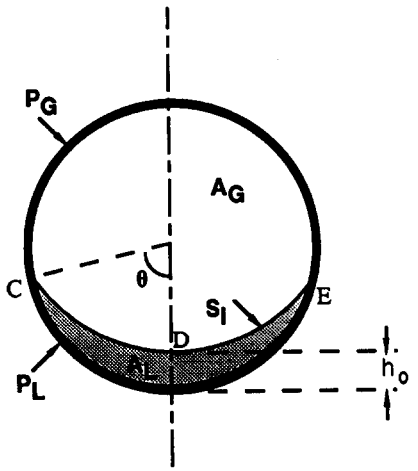

Figure 17. Schematic representation of horizontal gas–liquid stratified–atomization flow.

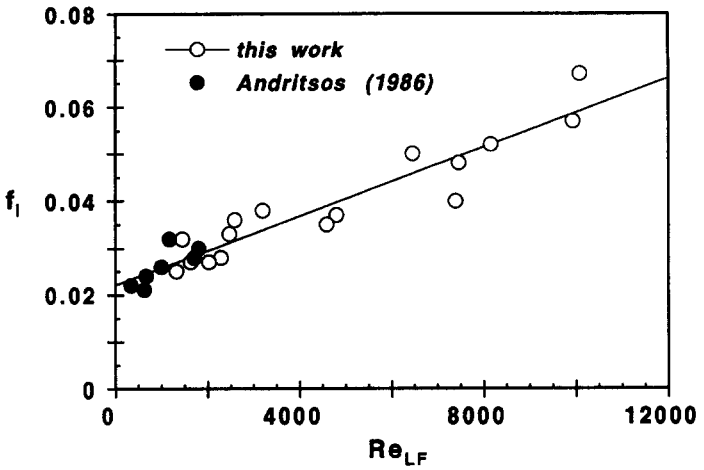

Figure 18. Correlation of interfacial friction factor with the liquid film Reynolds number.

of gas flow rate through the characteristic film length h_0 which is strongly influenced by U_G. However, an independent estimate of liquid film thickness h_0 is still required.

To explore another approach for predicting f_i we have considered the well known resistance formula for the completely rough regime (Schlichting 1960):

$$f_i = \frac{0.25}{\left(2\log_{10}\frac{R}{k_s} + 1.74\right)^2} \qquad [8]$$

where R is the tube radius and k_s is an apparent roughness. An effort is made here to determine an equivalent roughness of the gas–liquid interface by using independently obtained interfacial wave properties such as wave height and intermittency.

Hart *et al.* (1989), although they recognize the dependence of the liquid film "roughness" on the wave height and frequency, give a relation in which the intermittency of the waves is not taken into account. In the present study the calculated values of k_s normalized with respect to the pipe diameter are fitted satisfactorily (figure 19) by the following correlation in which the equivalent roughness is related to the wave characteristics:

$$\frac{k_s}{D} = 1.5\left(\frac{h_w}{D}\right) I^{0.17} \qquad [9]$$

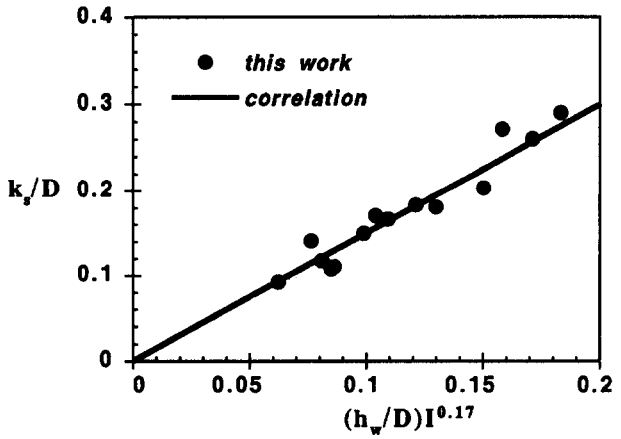

Figure 19. Apparent interface roughness (k_S) data correlated with liquid layer properties.

where h_w and I are large wave height and intermittency, respectively. It is noted that this correlation goes through zero as it would be required on physical grounds. It is also observed that the computed normalized roughness values are not far from those obtained for single-phase flow (e.g. Schlichting 1960). Obviously, for predictions, one needs expressions relating film characteristics to independently controlled flow parameters.

Some interesting observations can be made regarding the above computational procedure. It is noted first (table 1) that the ratio of wave height h_w over mean thickness at the bottom is roughly $(h_w/h_0) \approx 2$ and that the intermittency values from our tests vary in the range 0.05–0.35. However, $I^{0.17}$ varies between 0.60 and 0.84 in this range. To obtain rough estimates from [9] one could select an intermediate value $I^{0.17} = (0.2)^{0.17} \approx 0.75$ leading to

$$k_s \approx 2.3h_0 \qquad [10]$$

It will be pointed out that Hart *et al.* (1989) propose a similar expression for estimating k_s, i.e. $k_s \approx 2.3\delta$, where δ in their notation is an average liquid film thickness, not necessarily equal to the thickness h_0 employed in [10].

CONCLUDING REMARKS

With low viscosity fluids, by increasing the gas velocity above $U_G \approx 10$ m/s the wavy stratified flow changes considerably, entering a transition regime, i.e. stratified–atomization. Notable features of this regime include the appearance of disturbance waves, with a characteristic frequency ($\geqslant 1$ Hz) strongly dependent essentially only on U_G, the drastic change of the average gas–liquid interface profile from flat to "concave", and of course the onset of atomization.

Interpretation of the new film thickness data at $\Theta = 0°$ and 45° suggests that the dominant waves spread in the lateral direction and that their celerity is almost linearly increasing with U_G. Data on significant wave characteristics such as height (h_w) and intermittency (I) are reported and utilized to compute gas–liquid interfacial friction factor (f_i). These data are expected to be useful in future modelling of f_i and of liquid atomization.

The new result concerning time-averaged liquid-to-wall shear stress is that it tends to decrease in the lateral direction, i.e. away from the pipe bottom where the liquid film is thinner. More specifically, under constant flow conditions, the reduced mean shear stress in the lateral direction is associated with decreasing liquid film thickness. Film thickness and shear stress spectra display similarities, clearly showing the influence of waves on stress at the wall. Furthermore, they indicate that a certain class of dominant interface waves may not make its influence felt close to the wall if the liquid layer in that location is thick enough. Spectra of local liquid velocities at the wall (Paras & Karabelas 1992) show similar trends and support this interpretation. Probability densities of liquid thickness and of shear stress show surprising similarities, that are attributed to the liquid substrate at the wall on which the waves travel.

By taking into account the correct shape of the gas–liquid interface, improved estimates were obtained of liquid hold up and of the interfacial friction factor f_i. For the latter the pressure drop and shear stress measurements were employed. A linear relationship was obtained between f_i and liquid film Reynolds number, as also reported in previous studies. Finally, exploring the possibility of using statistical film characteristics to model interfacial friction, an expression was proposed for an equivalent roughness due to waviness.

It is noted that the axial wall stress was actually measured in these experiments. This is expected to be the dominant stress component under the prevailing relatively high velocities. However, in future studies the transverse stress component should be also measured to identify possible lateral velocities.

The type of experiments and the results presented here suggest that additional work on this flow regime may be quite rewarding in clarifying some key issues of separated two-phase flow, such as the spreading of liquid film on the wall in horizontal pipes and droplet atomization. Understanding the relative influence of these two mechanisms in promoting annular flow is certainly a topic of high priority.

Acknowledgement—Financial support from the Commission of European Communities under contracts JOUG-0005-C and JOU2-CT92-0108 is gratefully acknowledged.

REFERENCES

AGRAWAL, S. S., GREGORY, G. A. & GOVIER, G. W. 1973 An analysis of horizontal stratified two phase flow in pipes. *Can J. Chem. Engng* **51,** 280–286.

ANDRITSOS, N. 1986 Effect of pipe diameter and liquid viscosity on horizontal stratified flow. Ph.D. thesis, University of Illinois, Urbana, IL.

ANDRITSOS, N. 1992 Statistical analysis of waves in horizontal stratified gas–liquid flow. *Int. J. Mulitphase Flow* **18,** 465–473.

ANDRITSOS, N. & HANRATTY, T. J. 1987 Influence of interfacial waves in stratified gas–liquid flows. *AIChE Jl* **33,** 444–454.

BENDAT, J. S. & PIERSOL, A. G. 1986 *Random Data: Analysis and Measurement Procedures*, 2nd edn. Wiley–Interscience, New York.

CHEREMISINOFF, N. P. & DAVIS, E. J. 1979 Stratified turbulent–turbulent gas–liquid flow. *AIChE Jl* **25,** 48–56.

FUKANO, T., OUSAKA, A., MORIMOTO, T. & SEKOGUCHI, K. 1983 Air–water annular two-phase flow in horizontal tube. 2nd report. *Bull. ISME* **26,** 1387–1395.

GOVAN, A. H., HEWITT, G. F., OWEN, D. G. & BURNETT, G. 1989 Wall shear stress measurements in vertical air–water annular two-phase flow. *Int J. Multiphase Flow* **15,** 307–325.

HAGIWARA, Y., ESMAEILZADEH, E., TSUTSUI, H. & SUZUKI, K. 1989 Simultaneous measurement of liquid film thickness, wall shear stress and gas flow turbulence of horizontal wavy two-phase flow. *Int. J. Multiphase Flow* **15,** 421–431.

HANRATTY, T. J. & ENGEN, J. M. 1957 Interaction between a turbulent air stream and a moving water surface. *AIChE Jl* **3,** 299–304.

HART, J., HAMERSMA, P. J. & FORTUIN, J. M. H. 1989 Correlations predicting frictional pressure drop and liquid holdup during horizontal gas–liquid pipe flow with a small liquid holdup. *Int. J. Multiphase Flow* **15,** 947–964.

KOWALSKI, J. E. 1987 Wall and interfacial shear stress in stratified flow in a horizontal pipe. *AIChE Jl* **33,** 274–281.

MARTIN, C. J. & WHALLEY, P. B. 1983 Wall shear stress measurements in annular two-phase flow. Presented at *Int. Conf. On Physical Modelling Of Multiphase Flow*, Coventry, England, Paper G1.

MIYA, M., WOODMANSEE, D. E. & HANRATTY, T. J. 1971 A model for roll waves in gas–liquid flow. *Chem. Engng Sci.* **26,** 1915–1931.

PARAS, S. V. & KARABELAS, A. J. 1991 Properties of the liquid layer in horizontal annular flow. *Int. J. Multiphase Flow* **17,** 439–454.

PARAS, S. V. & KARABELAS, A. J. 1992 Measurements of local velocities inside thin liquid films in horizontal two-phase flow. *Exp. Fluids* **13,** 190–198.

SCHADEL, S. A. 1988 Atomization and deposition rates in vertical annular two-phase flow. Ph.D. thesis, University of Illinois, Urbana, IL.

SCHLICHTING, H. 1960 *Boundary Layer Theory*, 4th edn. McGraw–Hill, New York.

TAITEL, Y. & DUKLER, A. E. 1976 A model for predicting flow regime transitions in horizontal and near horizontal gas–liquid flow. *AIChE Jl* **22,** 47–55.

WU, H. L., POTS, B. F. M., HOLLENBERG, J. F. & MEERHOFF, R. 1987 Flow pattern transitions in two phase gas/condensate flow at high pressure in an 8-inch horizontal pipe. Presented at *3rd Int. Conf. On Multi-Phase Flow*, The Hague, The Netherlands, Paper A2.